# Pulse of the seafloor: Tidal triggering of microearthquakes at 9°50′N East Pacific Rise

D. F. Stroup,[1] D. R. Bohnenstiehl,[1,2] M. Tolstoy,[1] F. Waldhauser,[1] and R. T. Weekly[1]

[1]   Unequivocal evidence of tidal triggering is observed for microearthquakes ($-0.4$ to 2.0 $M_L$) recorded between October 2003 to April 2004 near 9°50′N on the East Pacific Rise (EPR). Although semidiurnal tidal stress changes are small (<2 kPa), seismicity exhibits a significant (>99.9%) nonrandom temporal distribution, with events occurring preferentially near times of peak extension. Due to the proximity of this site to an ocean tidal node, where changes in sea surface height are minimal, periodic stress changes are dominated by the solid Earth tide. In contrast, previous studies on the Juan de Fuca Ridge have shown microearthquake triggering to be a response to seafloor unloading during times of low ocean tide. The modulation of 9°50′N microearthquakes by small-amplitude periodic stresses is consistent with earthquake nucleation within a high stressing rate environment that is maintained near a critical state of failure by on-axis magmatic and hydrothermal processes. **Citation:** Stroup, D. F., D. R. Bohnenstiehl, M. Tolstoy, F. Waldhauser, and R. T. Weekly (2007), Pulse of the seafloor: Tidal triggering of microearthquakes at 9°50′N East Pacific Rise, *Geophys. Res. Lett.*, *34*, L15301, doi:10.1029/2007GL030088.

## 1.   Introduction

[2]   The role of periodic tidal stress variations in triggering seismicity has long been proposed [*Schuster*, 1897]. Studies focused on the origin times of global tectonic earthquakes, however, have often yielded conflicting results or shown little correlation [e.g., *Ambeh and Fairhead*, 1991; *Rydelek et al.*, 1992; *Johnston and Mauk*, 1972], though somewhat stronger correlations have been reported in volcanic regions [e.g., *Mauk and Johnston*, 1973; *Rydelek et al.*, 1988; *McNutt and Beavan*, 1981].

[3]   Early tidal studies were in part hindered by an inability to properly model the effect of ocean tidal loading (OTL), which may produce stress changes of greater amplitude ($\sim 10^4$ Pa) than the solid Earth tide ($\sim 10^3$ Pa) in some oceanic and coastal regions. Satellite altimetry now provides accurate information on the phase and amplitude of ocean tides throughout much of the global ocean [e.g., *Takanezawa et al.*, 2001]. Recent investigations have applied this improved knowledge to show that when tidal stresses are at their largest amplitudes and act in a direction favoring Coulomb failure, the origin times of moderate to large earthquakes may be influenced [*Tanaka et al.*, 2002; *Cochran et al.*, 2004]. Nonetheless, this effect is not universal and may vary temporally and spatially within a given region, presumably reflecting changes in the background state of stress within the lithosphere [*Tanaka*, 2006a, 2006b].

[4]   In the mid-ocean ridge setting, tidal processes are known to influence hydrothermal systems [e.g., *Schultz and Elderfield*, 1997]. Tidally induced pore-pressure may induce changes in hydrothermal fluid flow rates [*Glasby and Kasahara*, 2001; *Jupp and Schultz*, 2004; *Crone and Wilcock*, 2005] and modulate fluid exit temperatures [*Schultz and Elderfield*, 1997]. The hydrothermal and magmatic processes that support deep-sea vent systems also generate ubiquitous microearthquake activity. Studies on the Endeavor Segment [*Wilcock*, 2001] and near Axial Volcano [*Tolstoy et al.*, 2002] on the intermediate-spreading Juan de Fuca Ridge ($\sim 60$ mm/yr) have previously shown a correlation between the occurrence times of on-axis microearthquakes and tidal phase, with seismic events occurring preferentially at times of low ocean tide, when the height of the sea surface is at a minimum.

[5]   This study presents the first tidal triggering analysis of microearthquakes at a fast-spreading center ($\sim 110$ mm/yr), within a region where ocean tidal amplitudes are small relative to the Juan de Fuca Ridge and the local geology may create distinct thermal and mechanical conditions within the upper crust. Microearthquake data are obtained from ocean bottom seismic (OBS) sensors deployed in the vicinity of 9°50′N EPR between October 2003–April 2004. This deployment represents one of the longest continuous studies of ocean-bottom microearthquakes conducted in the mid-ocean ridge setting. Additionally, this site has been the focus of much interdisciplinary research since the immediate aftermath of an eruption was discovered in 1991 [*Haymon et al.*, 1991]. Following a build-up in seismic event rate during a 2.5+ year period, the area erupted again in January 2006, repaving much of the ridge crest [*Tolstoy et al.*, 2006a]. At the time of this study, the area hosted an array of high temperature vent sites, with circulation driven by the presence of a thin magma lens at a depth of $\sim 1.4$ km beneath the seafloor [*Kent et al.*, 1993].

## 2.   Microearthquakes at 9°50′N

[6]   Ocean-bottom data from six short-period vertical-channel seismometers and one hydrophone were recovered from a small-aperture array deployed in the vicinity of the 9°50′N vent field (Figure 1). Analyst-reviewed phase data from the 202-day deployment were used to locate earthquakes with the *Hypoinverse* algorithm [*Klein*, 2002]. The *hypoDD* double-difference procedure [*Waldhauser and*

---

[1]Lamont-Doherty Earth Observatory, Columbia University, Palisades, New York, USA.
[2]Now at Department of Marine, Earth, and Atmospheric Sciences, North Carolina State University, Raleigh, North Carolina, USA.
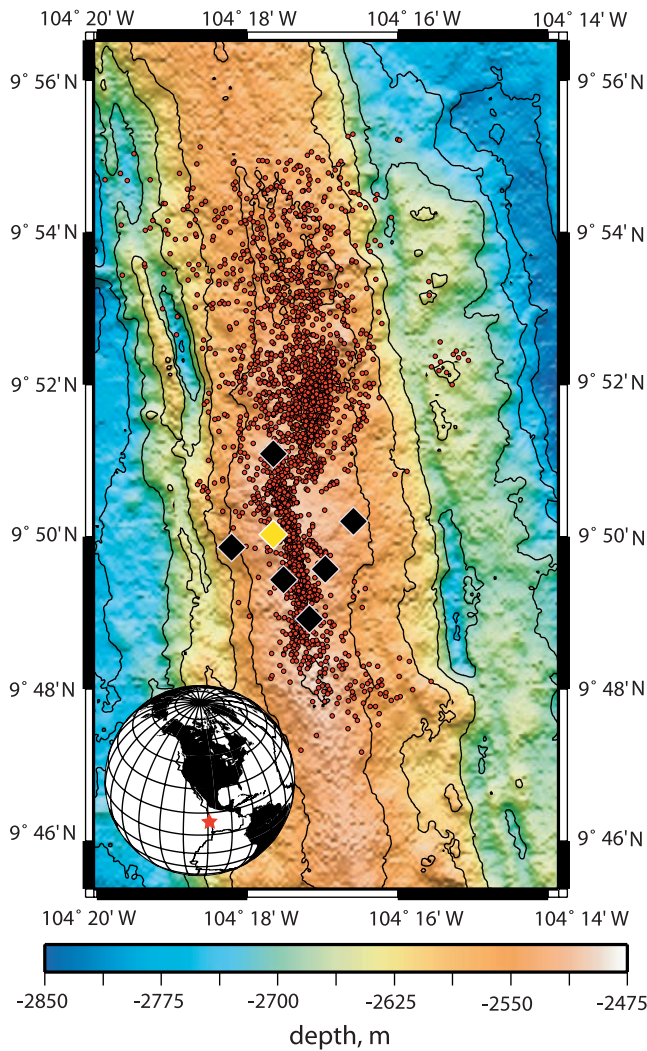
**Figure 1.** Bathymetric map of the East Pacific Rise showing relocated epicenters (red dots) of the 3,425 largest earthquakes studied along with the locations of the seismometers (black diamonds) and hydrophone sensor (yellow diamond) deployed during October 2003–April 2004.

*Ellsworth*, 2000] was then employed to produce a catalog of ~9000 relocated events within or near the OBS array (hypocentral data can be found at www.marine-geo.org). Local magnitude ($M_L$) estimates were derived from the measurement of peak displacement amplitude, with empirical distance and station magnitude corrections applied.

[7] This study examines the origin times of the 3,425 earthquakes with magnitudes greater than the completeness level of $M_L$ −0.4. The majority of events are tightly clustered within ~1 km of the axis, with additional activity to the northeast of the array (Figure 1). At depth, these microearthquakes are concentrated in a zone ~0.9–1.4 km below the seafloor [*Tolstoy et al.*, 2006b], where the background stress field is controlled by hydrothermal cooling-induced contraction [*Sohn et al.*, 1999, 2004] and the inflation (or deflation) of the axial magma lens.

## 3. Earth and Ocean Tides

[8] Modeled ocean tidal data were obtained using the NAO99.b model [*Matsumoto et al.*, 2000]. The NAO99.b model calculates pure ocean tide with respect to the ocean floor based on five years of TOPEX/POSEIDON altimetry data and the long-period ocean tide map of *Takanezawa et al.* [2001]. The model represents 16 major short-period tidal constituents and has a spatial resolution of $0.5° \times 0.5°$. Ocean tides at this location (9°50′N, 104°17′W) range between −0.4 to 0.2 m (Figure 2a).

[9] Strains induced by OTL and Earth tides were estimated using the GOTIC2 model, which utilizes the mass-loading Green's function for strain and is based on the 1066A Earth model [*Matsumoto et al.*, 2001]. Short-period tidal constituents from NAO99.b and five long-period constituents based on loading tides are incorporated. Within the shallow depth extent of microearthquake activity (<1.4 km), the mode of failure is predicted to be tensile or mixed-mode [e.g., *Bohnenstiehl and Carbotte*, 2001]. Therefore, this study focuses on the variations in volumetric stress ($\sigma_v$), which is estimated from the GOTIC2-derived volumetric strain, assuming a crust with $V_p$ = 6.5 km/s, $V_s$ = 3.5 km/s, $\rho$ = 2800 kg/m$^3$. The modeled amplitude of $\sigma_v$ ranges between ±1.0 kPa for OTL and ±2.5 kPa for Earth tide (Figure 2a).

## 4. Tidal Correlations

[10] A visual assessment of the occurrence of micro-earthquakes relative to the combined stress resulting from OTL and Earth tides suggests that microearthquakes are occurring preferentially at or near times of peak volumetric extension (Figure 2b). The periodic stress changes associated with OTL and Earth tide are dominantly out of phase (Figure 2a), with troughs in OTL (compression) exhibiting a small average lag relative to peaks in Earth tide stress (extension). The combined stress field therefore typically reaches maximum extension ~1 hour after the time of peak ocean tidal height, with larger amplitude Earth tide stresses counteracting the ocean loading effect.

[11] To further quantify these observations, the tidal phase of earthquake origin times is calculated with respect to sea surface height, OTL, Earth tide stress, and the combined effects of both OTL and Earth tide stress. Tidal series peaks (i.e. high tide for sea surface height and peak extension for all volumetric stresses) are assigned a 0° phase, and the subsequent and preceding troughs (i.e. low tide for sea surface height and peak compression for all volumetric stresses) are assigned a phase of ±180° (Figure 3a). Relative to the various tidal datasets, micro-earthquake origin times display mean phase angles ($\bar{\theta}$) of 38.3° (sea surface height), −131.9° (OTL $\sigma_v$), 5.7° (Earth tide $\sigma_v$), and −1° (combined OTL and Earth tide $\sigma_v$) (Figure 3b and Table S1[1]). Similarly, phase angles for the combined OTL and Earth tide $\sigma_v$ exhibit the minimum variance, with larger mean resultant vector lengths ($\bar{R}$) and von Mises concentration parameters ($K$), which indicate how closely the phasors cluster around $\bar{\theta}$ [*Jones*, 2006]
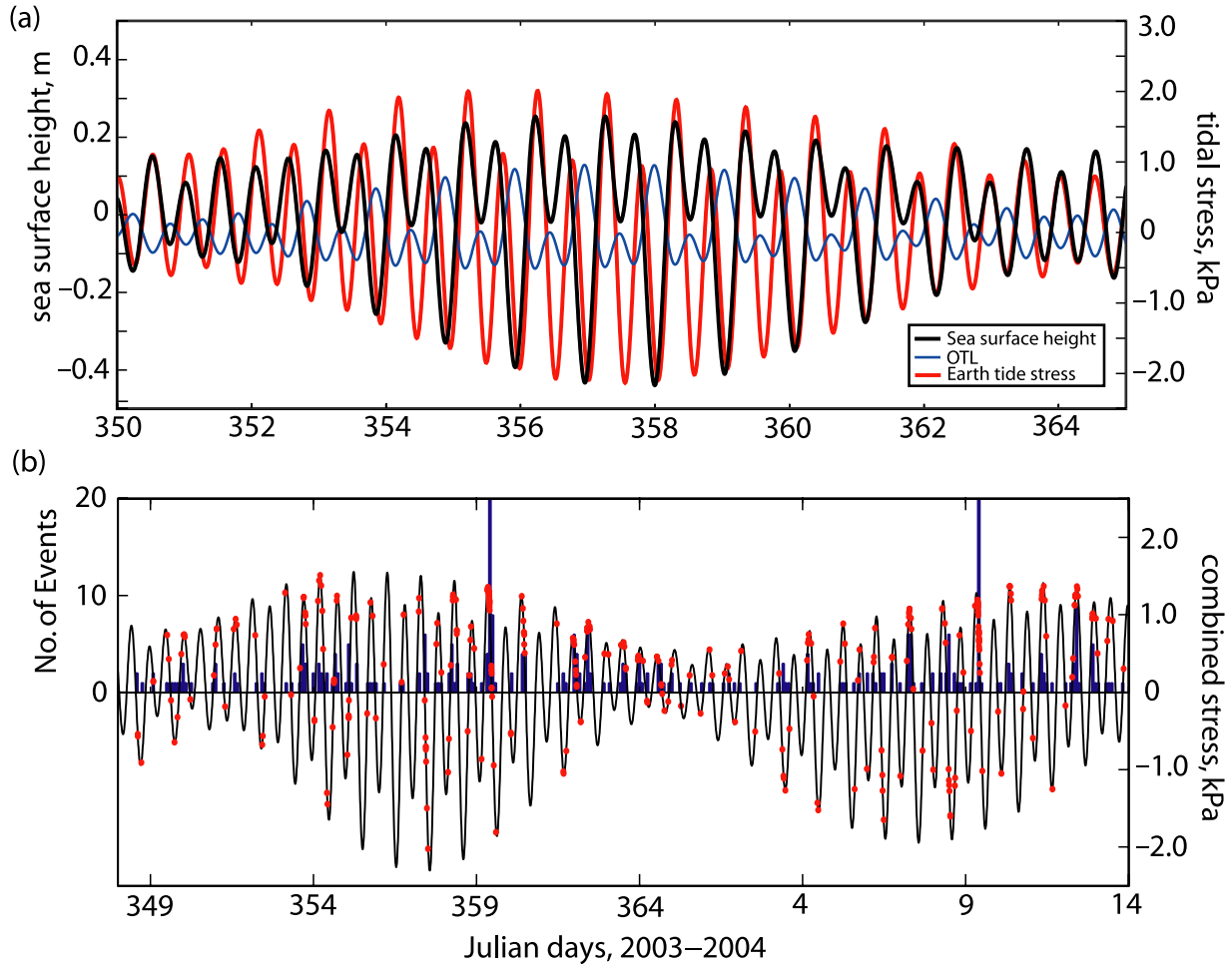
---

**Figure 2.** (a) Sea surface height (in black) shown with Earth tide stress (in red) and ocean tidal loading (OTL) (in blue) during a sixteen-day period from December 15–31, 2003 (Julian days 350–365). Earth tide stresses are larger in amplitude and typically out of phase relative to OTL. (b) Thirty-one day earthquake histogram (blue bars) from December 14, 2003 to January 14, 2004 (Julian days 349-14) in 2 hour bins with the combined OTL and Earth tide stress (solid curve) and corresponding microearthquakes (red dots) superimposed. Positive values of stress indicate extension.

(Table S1). Earthquake events, therefore, correlate most closely with times of peak (0° phase) extension. The phase angles, however, are not perfectly symmetric, with 1,793 out of 3,425 earthquakes occurring during times of increasing ($-180° < \theta < 0°$), rather than decreasing ($0° < \theta < 180°$), volumetric stress. A simple binomial test shows that the probability of obtaining this result by chance is <4% (see discussion in Text S1).

[12] The Schuster test [*Schuster*, 1897; *Emter*, 1997] quantifies the probability that a given set of phase angles,

relating earthquake origin times to a specific temporal periodicity (the tidal series in this case), are randomly distributed about the unit circle. The probability $p$ that the earthquake phase distribution is random is given by:

$$p = \exp\left(\frac{-R^2}{N}\right), \tag{1}$$

where $R$ is the sum of the unit phasors representing the direction of each phase angle and $N$ is the total number of

**Figure 3.** (a) Definition of a phase angle. The peak of tidal stress is assigned a phase angle of 0°, and the surrounding tidal troughs are assigned a phase angle of ±180°. For example, an earthquake (red dot) occurring directly between a peak and a trough is assigned a phase angle of 90°. After *Tanaka et al.* [2002]. (b) Rose diagrams illustrating the phase distribution of microearthquakes relative to sea surface height, and the volumetric stress ($\sigma_v$) associated with ocean tidal loading (OTL), Earth tide, and the combined OTL and Earth tide. (c) The frequency of earthquakes (hr$^{-1}$) as a function of the combined OTL and Earth tide $\sigma_v$ in 0.23 kPa bins. The plot shows the full dataset of earthquakes (blue crosses) and declustered earthquakes (red triangles). Dashed line shows the mean earthquake frequency within the full dataset at times of compression.
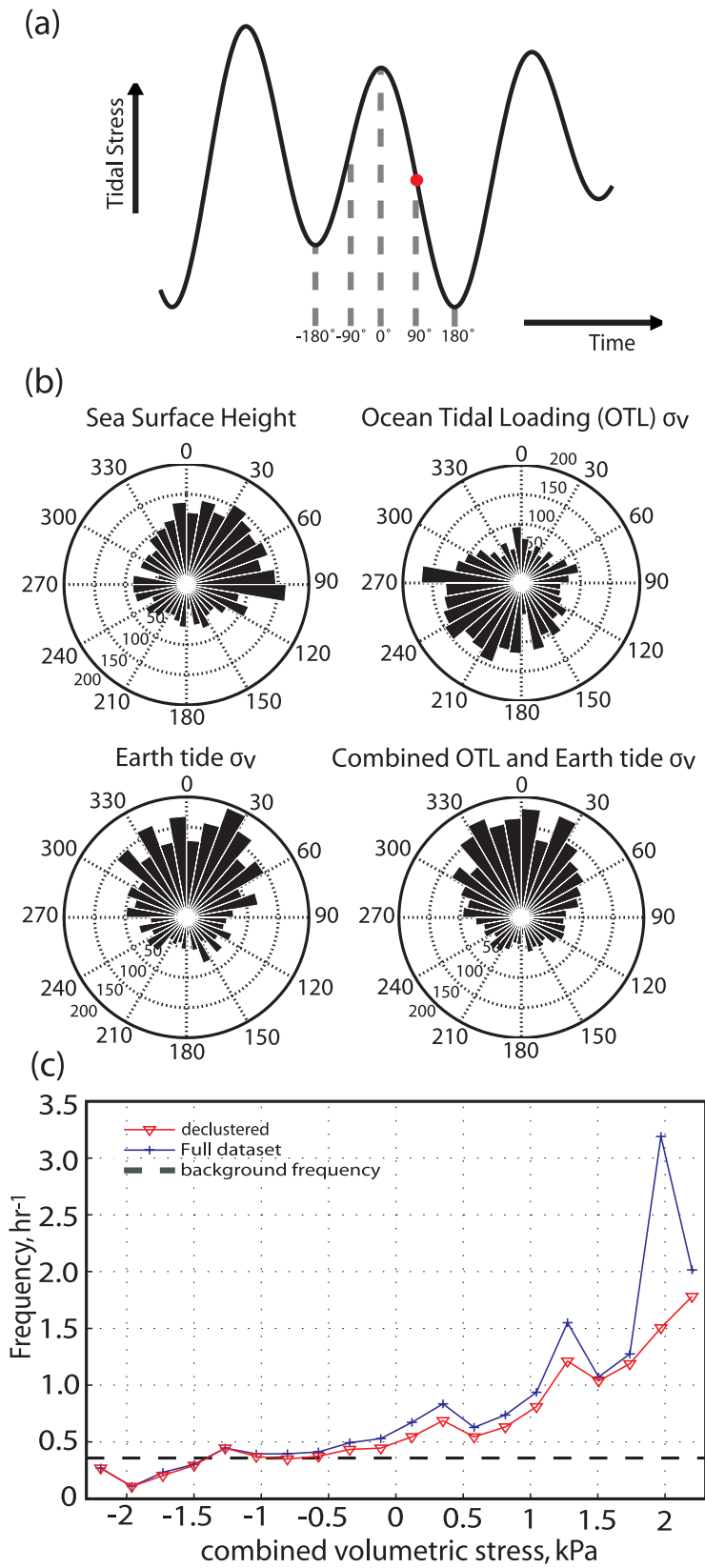
**Figure 3**

microearthquake events ($N$ = 3,425). A $p$-value $\leq$ 0.05 (95% confidence) is generally considered as the threshold of statistical significance. In this study, the values of $p$ are found to be on the order of $\sim10^{-10}$ (Table S1), indicating that earthquake origin times clearly occur at non-random times with respect to tidal phase; that is, earthquakes are unequivocally correlated with a particular tidal phase.

[13] The presence of one or more large earthquake sequences of short duration may lead to statistical bias when calculating the Schuster test because many micro-earthquakes will occur at approximately the same tidal phase. To account for this, we use a single-link cluster algorithm with a combined space-time metric to identify and remove the dominant earthquake sequences (aftershocks and swarms) from the dataset [e.g., *Davis and Frohlich*, 1991; *Bohnenstiehl et al.*, 2002]. The $p$-value is then recalculated for the declustered population (Table S1). A range of parameter values were tested in applying this procedure, all of which produced similar results. The declustering presented here gives equal weight to a 1 km spatial separation and a 0.2 day temporal separation, and defines sequences using a threshold link value equal to the median link-length within the catalog. The largest fifteen earthquake sequences were removed from the data, consisting of 528 earthquakes in total or $\sim15\%$ of the catalog. The population remains significantly (>99.9%) nonrandom (Table S1).

[14] Examination of the frequency of earthquakes (hr$^{-1}$) compared to the combined OTL and Earth $\sigma_v$ amplitude (Figure 3c) indicates that the rate of earthquake activity at times of compression displays a mean frequency of 0.4 event/hr, but as the amplitude of extensional stress increases, the microearthquake frequency increases to a maximum rate of $\sim2$ event/hr ($\sim5$ times the background frequency) for stress amplitudes >2 kPa. The shape of this frequency histogram is consistent with that reported by *Wilcock* [2001]; however, even at the largest extensional stress observed on the Juan de Fuca Ridge (>20 kPa), the rate of earthquake activity was only increased by a factor of $\sim2$ relative to the background frequency.

[15] To further test the significance of these results, the percentage of excess events ($N_{ex}$) at times of encouraging stress is calculated in each tidal cycle [*Cochran et al.*, 2004]:

$$N_{ex} = \frac{N_{enc} - \dfrac{N_t}{2}}{N_t} \times 100, \qquad (2)$$

where $N_{enc}$ is the number of events with $-90° < \theta < 90°$ and $N_t$ is the total number of earthquakes. If earthquakes occur randomly, the number of events at times when the stress field encourages failure ($-90° < \theta < 90°$) should equal the number of events during the other half of the tidal cycle. In Figure S1, the parameter $N_{ex}$ is plotted as a function of the peak-to-peak amplitude of the tidal stress, with vertical error bars representing the standard error within each bin. The data show a positive correlation between peak-to-peak tidal stress and the percentage of excess events occurring during times of encouraging stress. The significance of these observations can be evaluated against a binomial model. For each stress bin, the binomial cumulative distribution

function is used to estimate the confidence limits for the observed $N_{ex}$ and $N_{enc}$ values (results are summarized in Table S2). For tidal cycles with peak-to-peak stress amplitudes >0.7 kPa, the observed number of excess events occurring during times of encouraging stress is >99.99% significant relative to the binomial model.

## 5. Discussion and Conclusions

[16] The triggering of microearthquakes beneath the 9°50′N vent field occurs during times of peak extension. This observation is consistent with shorter-duration OBS studies on the Juan de Fuca Ridge [*Wilcock*, 2001; *Tolstoy et al.*, 2002]. At these northeast Pacific spreading centers, however, stress changes are strongly modulated by OTL, with periods of maximum extension occurring near times of low ocean tide when the seafloor was unloaded. Earthquakes at 9°50′N EPR more closely track Earth tide induced stress changes, which are out of phase with OTL and exhibit amplitudes that are $\sim2.5$ times larger than OTL. The variable contribution of OTL and Earth tide between these distant sites reflects an order of magnitude difference in the amplitude of the ocean tidal signals, with maximum sea surface heights of $\sim0.2$ m on the EPR versus $\sim2$ m on the Juan de Fuca Ridge. In his detailed 1976 investigation of swarms, *Klein* [1976] suggested that the spatially variable magnitude of OTL would lead to these types of site-specific behaviors. At that time, however, little was known about the phase and amplitude of tides in the deep ocean and the process could not be accurately modeled.

[17] The amplitude of tidal stress changes is much smaller than the tensile strength of basalt ($\sim2$ MPa) and is therefore not the underlying process causing cracking and seismicity within the region. Rather, the removal of heat and subsequent thermal contraction, combined with the concentration of stress in the vicinity of the axial magma chamber (AMC), as well as the tectonic stresses associated with plate spreading, create a critically-stressed upper crust that is susceptible to tidal influence. These processes control the background rate of seismicity, with tidal stress changes modulating the timing of earthquakes.

[18] The experimental results of *Beeler and Lockner* [2003] suggest that seismicity should correlate with the amplitude and frequency of periodic stress changes, if their period exceeds the duration of earthquake nucleation. Given that the nucleation time is proportional to the ratio of normal stress to stressing rate, it is estimated to be on the order of a year or more in most tectonic environments [*Beeler and Lockner*, 2003]. Consequently, only a weak correlation with semidiurnal tidal stressing is predicted under these conditions. At 9°50′N EPR, however, hydrothermal cooling and magmatic inflation may elevate the background stressing rate within the shallow lid above the AMC by $2-4$ orders of magnitude [*Sohn et al.*, 1999, 2004]. The elevated background stressing rate will result in a proportional reduction of earthquake nucleation time and will generate an environment more prone to tidal triggering.

# References

Ambeh, W. B., and J. D. Fairhead (1991), Regular, deep seismicity beneath Mt. Cameroon volcano—Lack of evidence for tidal triggering, *Geophys. J. Int.*, *106*, 287–291.

Beeler, N. M., and D. A. Lockner (2003), Why earthquakes correlate weakly with the solid Earth tides: Effects of periodic stress on the rate and probability of earthquake occurrence, *J. Geophys. Res.*, *108*(B8), 2391, doi:10.1029/2001JB001518.

Bohnenstiehl, D. R., and S. M. Carbotte (2001), Faulting patterns near 19°30′S on the East Pacific Rise: Fault formation and growth at a super-fast spreading center, *Geochem. Geophys. Geosyst.*, *2*(9), doi:10.1029/2001GC000156.

Bohnenstiehl, D. R., M. Tolstoy, R. P. Dziak, C. G. Fox, and D. K. Smith (2002), Aftershock sequences in the mid-ocean ridge environment: An analysis using hydroacoustic data, *Tectonophysics*, *354*, 49–70.

Cochran, E. S., J. E. Vidale, and S. Tanaka (2004), Earth tides can trigger shallow thrust fault earthquakes, *Science*, *306*, 1164–1166.

Crone, T. J., and W. S. D. Wilcock (2005), Modeling the effects of tidal loading on mid-ocean ridge hydrothermal systems, *Geochem. Geophys. Geosyst.*, *6*, Q07001, doi:10.1029/2004GC000905.

Davis, S. D., and C. Frohlich (1991), Single-link cluster-analysis, synthetic earthquake catalogs, and aftershock identification, *Geophys. J. Int.*, *104*, 289–306.

Emter, D. (1997), Tidal triggering of earthquakes and volcanic events, in *Tidal Phenomena*, edited by S. Bhattacharji et al., pp. 293–309, Springer, New York.

Glasby, G. P., and J. Kasahara (2001), Influence of tidal effects on the periodicity of earthquake activity in diverse geological settings with particular emphasis on submarine hydrothermal systems, *Earth Sci. Rev.*, *52*, 261–297.

Haymon, R. M., D. J. Fornari, M. H. Edwards, S. Carbotte, D. Wright, and K. C. MacDonald (1991), Hydrothermal vent distribution along the East Pacific Rise crest (9°09′–54′N) and its relationship to magmatic and tectonic processes on fast-spreading mid-ocean ridges, *Earth Planet. Sci. Lett.*, *104*, 513–534.

Johnston, M. J., and F. J. Mauk (1972), Earth tides and the triggering of eruptions from Mt. Stromboli, Italy, *Nature*, *239*, 266–267.

Jones, T. A. (2006), MATLAB function to analyze directional (azimuthal) data—I: Single-sample inference, *Comput. Geosci.*, *32*, 166–175.

Jupp, T. E., and A. Schultz (2004), A poroelastic model for the tidal modulation of seafloor hydrothermal systems, *J. Geophys. Res.*, *109*, B03105, doi:10.1029/2003JB002583.

Kent, G. M., A. J. Harding, and J. A. Orcutt (1993), Distribution of magma beneath the East Pacific Rise between the Clipperton Transform and 9°17′ Deval from forward modeling of common depth point data, *J. Geophys. Res.*, *98*, 13,945–13,969.

Klein, F. W. (1976), Earthquake swarms and semidiurnal solid earth tide, *Geophys. J. R. Astron. Soc.*, *45*, 245–295.

Klein, F. W. (2002), User's guide to HYPOINVERSE2000, a Fortran program to solve for earthquake locations and magnitudes, *U.S. Geol. Surv. Open File Rep.*, *02-172*, 123 pp.

Matsumoto, K., T. Takanezawa, and M. Ooe (2000), Ocean tide models developed by assimilating TOPEX/POSEIDON altimeter data into hydrodynamical model: A global model and a regional model around Japan, *J. Oceanogr.*, *56*, 567–581.

Matsumoto, K., T. Sato, T. Takanezawa, and M. Ooe (2001), GOTIC2: A program for computation of oceanic tidal loading effect, *J. Geod. Soc. Jpn.*, *47*, 243–248.

Mauk, F. J., and M. J. Johnston (1973), Triggering of volcanic eruptions by Earth tides, *J. Geophys. Res.*, *78*, 3356–3362.

McNutt, S. R., and R. J. Beavan (1981), Volcanic earthquakes at Pavlof Volcano correlated with the solid earth tide, *Nature*, *294*, 615–618.

Rydelek, P. A., P. M. Davis, and R. Y. Koyanagi (1988), Tidal triggering of earthquake swarms at Kilauea Volcano, Hawaii, *J. Geophys. Res.*, *93*, 4401–4411.

Rydelek, P. A., I. S. Sacks, and R. Scarps (1992), On tidal triggering of earthquake at Campi Flegrei, Italy, *Geophys. J. Int.*, *109*, 125–137.

Schultz, A., and H. Elderfield (1997), Controls on the physics and chemistry of seafloor hydrothermal circulation, *Philos. Trans. R. Soc. London*, *355*, 387–425.

Schuster, A. (1897), On lunar and solar periodicities of earthquakes, *Proc. R. Soc. London*, *61*, 455–465.

Sohn, R. A., J. A. Hildebrand, and S. C. Webb (1999), A microearthquake survey of the high-temperature vent field on the volcanically active East Pacific Rise (9°50′N), *J. Geophys. Res.*, *104*, 25,367–25,377.

Sohn, R. A., A. H. Barclay, and S. C. Webb (2004), Microearthquake patterns following the 1998 eruption of Axial Volcano, Juan de Fuca Ridge: Mechanical relaxation and thermal strain, *J. Geophys. Res.*, *109*, B01101, doi:10.1029/2003JB002499.

Takanezawa, T., K. Matsumoto, M. Ooe, and I. Naito (2001), Effects of the period ocean tides on Earth rotation, gravity and crustal deformation predicted by global barotropic model—Period from Mtm to Sa, *J. Geod. Soc. Jpn.*, *47*, 545–550.

Tanaka, S. (2006a), Tidal triggering of earthquakes in the subducting Phillippine Sea plate beneath the locked zone of the plate interface in the Tokai region, Japan, *Tectonophysics*, *417*, 69–80.

Tanaka, S. (2006b), Tidal triggering of earthquakes precursory to the 2004 Mw = 9.0 off Sumatra earthquake, paper presented at the 4th International Workshop on Statistical Seismology, Grad. Univ. for Adv. Stud., Kanagawa, Japan, 9–13 Jan.

Tanaka, S., M. Ohtake, and H. Sato (2002), Evidence for tidal triggering of earthquakes as revealed from statistical analysis of global data, *J. Geophys. Res.*, *107*(B10), 2211, doi:10.1029/2001JB001577.

Tolstoy, M., F. L. Vernon, J. A. Orcutt, and F. K. Wyatt (2002), Breathing of the seafloor: Tidal correlations of seismicity at Axial Volcano, *Geology*, *30*, 503–506.

Tolstoy, M., et al. (2006a), A seafloor spreading event captured by seismometers, *Science*, *314*, 1920–1922, doi:10.1126/science.1133950.

Tolstoy, M., F. Waldhauser, D. R. Bohnenstiehl, R. T. Weekly, W. Kim (2006b), Microearthquake patterns within a fast-spreading ridge hydrothermal system at 9°50′N on the East Pacific Rise, *EOS Trans. AGU*, Fall Meet. Suppl., *87*(52), Abstract B33D-04.

Waldhauser, F., and W. L. Ellsworth (2000), A double-difference earthquake location algorithm: Method and application to the northern Hayward fault, California, *Bull. Seismol. Soc. Am.*, *6*, 1353–1368.

Wilcock, W. (2001), Tidal triggering of microearthquakes on the Juan de Fuca Ridge, *Geophys. Res. Lett.*, *28*, 3999–4002.

————————————

D. R. Bohnenstiehl, Department of Marine, Earth, and Atmospheric Sciences, North Carolina State University, Campus Box 8208, Raleigh, NC 27695, USA.

D. F. Stroup, M. Tolstoy, F. Waldhauser, and R. T. Weekly, Lamont-Doherty Earth Observatory, Columbia University, 61 Route 9W, Palisades, NY 10964, USA. (danielle@ldeo.columbia.edu)